Plant Biotechnology Journal
Open Access

Plant Biotechnology Journal (2023) **21**, pp. 460–462 doi: 10.1111/pbi.13978

Brief Communication

Two determinants influence CRY2 photobody formation and function

Ling Ma[1], Hanli Jia[1], A-lan Shen[1], Junya Ding[1], Xiaoyu Wang[1], Jing Wang[1], Jiajia Wan[1], Junjie Yan[1], Delin Zhang[1], Xu Dong[2,*] and Ping Yin[1,*]

[1]*National Key Laboratory of Crop Genetic Improvement, Hubei Hongshan Laboratory, Huazhong Agricultural University, Wuhan, China*
[2]*Innovation Academy for Precision Measurement Science and Technology, Chinese Academy of Sciences, Wuhan, China*

Received 11 October 2022;
revised 3 December 2022;
accepted 8 December 2022.
**Correspondence* (Tel +86-027-87285221; fax +86-027-87288920; email yinping@mail.hzau.edu.cn (P.Y.) and Tel +86-027-87197358; fax +86-027-87199543; email dongxu@wipm.ac.cn (X.D.))

Keywords: photoreceptors, photobody, cryptochromes, phase separation, NMR.

In plants, cryptochromes (CRYs) are blue light receptors that regulate various developmental progress. Photoactivated CRYs undergo a series of molecular events, including tetramerization, photobody formation and interactions with signal-transduction proteins, to transduce blue light signals (Wang and Lin, 2020). Owing to their light-induced self-oligomerization and protein-interacting features, CRYs are widely used in optogenetics (Seong and Lin, 2021; Figure 1a). Photoactivated CRY2 forms photobodies through phase separation (Wang *et al.*, 2021). The CRY2 C-terminal extension (CCE) domain and its phosphorylation are required for maintaining the liquid property of CRY2 photobody (Wang *et al.*, 2021). However, the residues essential for CRY2 phase separation and the underlying mechanism remain elusive.

Consistent with the previous report (Wang *et al.*, 2021), our results also suggest that photoactivated CRY2 undergoes phase separation to form photobodies (Figure 1b–f and Figure S1). We then investigated the determinants that influence CRY2 photobody formation and function. CRY2 contains an N-terminal photolyase homology region (PHR) domain (residues 1–489) and a CRY CCE domain (residues 490–612). In line with the previous findings (Wang *et al.*, 2021), we also found that the CCE domain modulates the size and property of CRY2 phase separation (Figures S2 and S3). We divided the CCE into 20 parts and explored which residues influence photobody formation through alanine-substitution analyses (Figure S4A). Except for $CRY2^{M9\text{-}A}$ and $CRY2^{M11\text{-}A}$, the rest 18 mutants formed photobodies similar to the ones observed in $CRY2^{WT}$ (Figure S4B). We further fused the TALE-effector NLS RVKRPRTR (T-NLS) to $CRY2^{M9\text{-}A}$ and $CRY2^{M11\text{-}A}$ as the CRY2 nuclear localization sequence (NLS) was partially disrupted in $CRY2^{M9\text{-}A}$ and $CRY2^{M11\text{-}A}$. The sizes of $CRY2^{M9\text{-}A}$+T-NLS and $CRY2^{M11\text{-}A}$+T-NLS speckles were smaller than those of $CRY2^{WT}$ (Figure S4C), suggesting that the CRY2 NLS (541–557) might modulate CRY2 phase separation. $CRY2^{\Delta N538\text{-}R557}$+T-NLS (N538-R557 truncation) formed small speckles in the nucleus (Figure 1g and Figure S4D), which is similar to those observed for $CRY2^{PHR}$+T-NLS (Figure S2). These together suggest that the CRY2 NLS not only mediates nuclear importation but also affects photobodies size, marking a step forward in understanding the specific residues that modulates the previously discovered CRY2 phase separation (Wang *et al.*, 2021).

We further explored how the CCE domain modulates CRY2 phase separation. Consistent with a previous report (Partch *et al.*, 2005), our nuclear magnetic resonance (NMR) results suggest that the CCE domain is highly dynamic and flexible (Figure S5). As phase separation can be driven by multivalent interactions, we investigated the inter-molecular interactions between CCE domains via NMR (Figures S6 and S7). The observed chemical shift perturbations indicate that the CCE G558-C611 region underwent slight conformational changes upon blue light irradiation (Figure 1h and Figure S7D), which is in line with a previous report (Partch *et al.*, 2005). Signal intensities of many CCE residues (including V535, V543, E546, G558 and V579) decreased, possibly owing to the weak CCE-CCE and/or CCE-PHR-tetramer interactions of the photoactivated CRY2 (Figure 1i). Furthermore, the paramagnetic relaxation enhancement profiles indicated that the Ipara/Idia ratios decreased around CCE residues G511-F559 and S587-T604 after blue light illumination (Figure 1j and Figure S8). Taken together, these data suggest the occurrence of intermolecular CCE-CCE interactions in CCE G511-F559 and S587-T604 regions. Many of these residues were within or close to the CCE N538-R557 region, which have a role in regulating CRY2 photobody size (Figure 1g). Thus, we speculate that these interactions might contribute to phase separation of photoactivated CRY2. Whether phosphorylation affects the intermolecular interactions between the CCE domains remains to be elucidated.

Cysteines can modulate phase separation (Wang *et al.*, 2019); we wondered whether CRY2 cysteines participate in photobody formation. Eight and three cysteines were found in the PHR and CCE domains, respectively. We generated the $CRY2^{8Cmut}$, $CRY2^{3Cmut}$ and $CRY2^{11Cmut}$ mutants harbouring the mutations for the 8 PHR cysteines, 3 CCE cysteines and all 11 cysteines, respectively (Figure S9A). These mutants retained the photoactivated tetramerization and photoreduction capacity (Ma *et al.*, 2020) (Figure S9B,C), suggesting that mutating these cysteines had little impact on CRY2 structure. However, $CRY2^{8Cmut}$ and $CRY2^{11Cmut}$ completely lost the photobody formation capability (Figure 1k and Figure S9D). Moreover, compared to PHR^{WT}, the blue light-induced soft gel-like phase transition of PHR^{8Cmut} was significantly decreased in vitro (Figure S9E), suggesting that the PHR cysteines play crucial roles in CRY2 phase separation. Four of the eight cysteines locate on the surface of the photoactivated CRY2 tetramer (Figure S9F); we thus speculate that these residues might play roles in sensing the redox state of surrounding conditions and modulating the oligomerization of CRY2 tetramer. How these cysteines influence

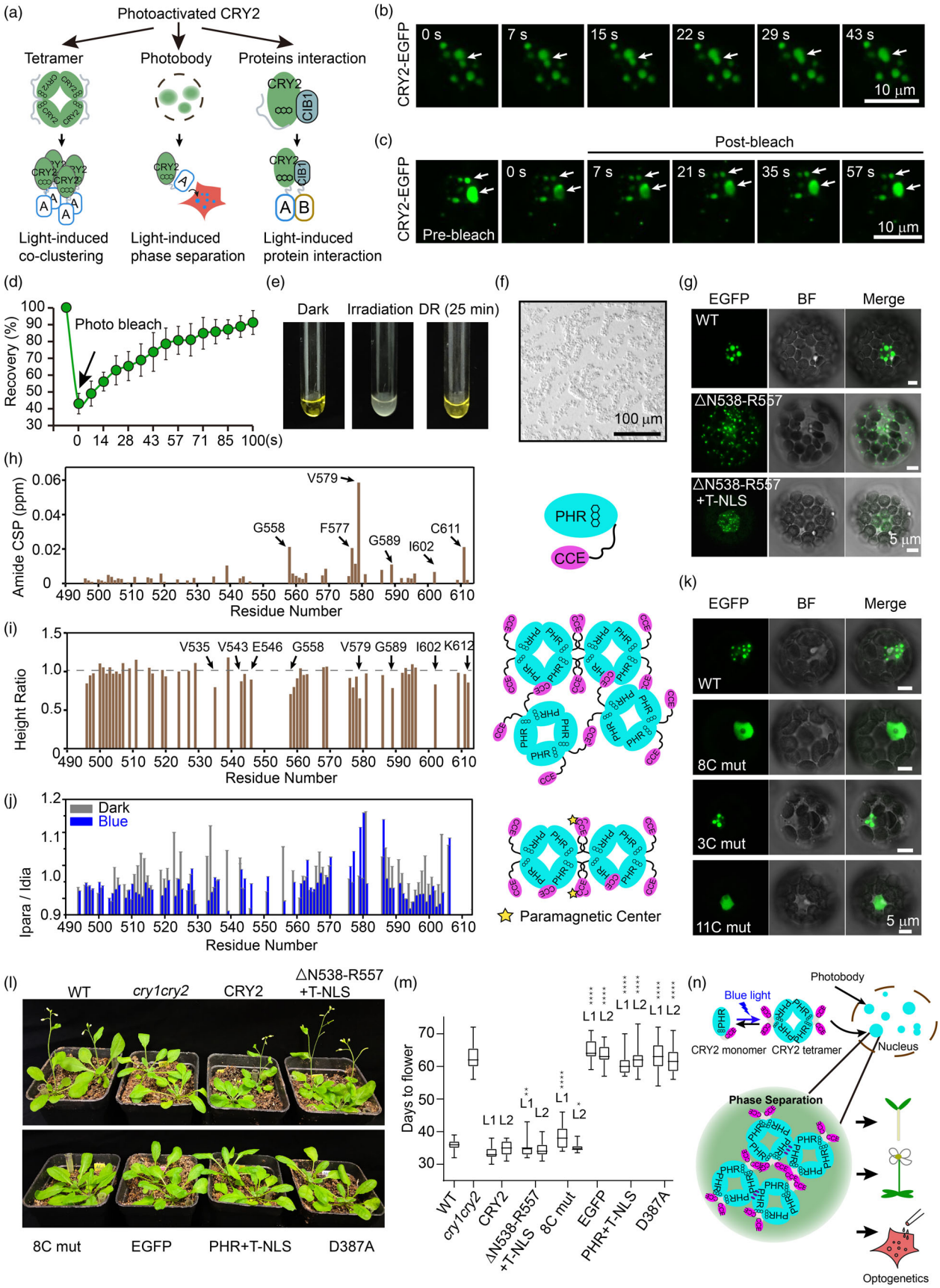

Figure 1 The N538-R557 region in the C-terminal extension (CCE) domain and Cysteines in the PHR domain influence CRY2 photobody formation and function. (a) cryptochromes (CRYs) are widely used in optogenetics. (b) Fusion observations of two CRY2-EGFP photobodies in *Arabidopsis* protoplasts. $n = 3$. (c) FRAP of CRY2-EGFP photobodies in *Arabidopsis* protoplasts. (d) Averaged FRAP recovery curve of CRY2-EGFP photobodies in (c). Data are expressed as the mean ± SD. $n = 5$. (e) Purified CRY2 protein (300 μM) undergoes phase transition upon blue light treatment. Turbid CRY2 solution reverts to clear in darkness. DR, dark reversion. (f) Bright-field image of photoactivated turbid CRY2 solution in (e). (g) Speckles morphology of $CRY2^{\Delta N538\text{-}R557}$-EGFP and $CRY2^{\Delta N538\text{-}R557}$-EGFP+T-NLS in *Arabidopsis* protoplasts. BF: bright field. (h) Chemical shift perturbations for the backbone amide proton and nitrogen atoms of PHR-^{15N}CCE in darkness and under blue light. (i) The peak height ratios of PHR-^{15N}CCE in darkness and under blue light. Columns with ratio below 1.0 (dashed line) indicate residues with decreased signal intensities upon blue light irradiation. (j) Paramagnetic relaxation enhancement analysis of sortase ligated PHR-CCE proteins in darkness and under blue light. (k) Representative images showing the photobodies of $CRY2^{WT}$, $CRY2^{3Cmut}$, $CRY2^{8Cmut}$ and $CRY2^{11Cmut}$ in *Arabidopsis* protoplasts. (l) Images of 36-day-old transgenic plants grown in long-day conditions. (m) Days to flowering of transgenic plants. L1:line1; L2: line2. Differences between indicated genotypes and 'CRY2 L1' are analysed by two-tailed paired *t*-tests. Lines that show significantly delayed flowering are indicated by *. *$P < 0.05$; **$P < 0.01$; ****$P < 0.0001$. Data are presented as mean ± SD. $n \geq 20$. (*n*), Proposed mechanism and functions for CRY2 photobody formation.

CRY2 phase separation and function and whether the redox equilibrium of blue light-irradiated living cells modulates CRY2 photobody formation await further investigation.

To investigate whether CRY2 photobody formation influences its physiological functions, we introduced individual CRY2-EGFP, $CRY2^{8Cmut}$-EGFP, $CRY2^{\Delta N538\text{-}R557}$-EGFP+T-NLS, $CRY2^{PHR}$-EGFP+T-NLS, $CRY2^{D387A}$-EGFP (unable to perceive blue light) or EGFP in the *cry1cry2 Arabidopsis* background and examined the hypocotyl length and flowering time of the transgenic plants. Under blue light treatment, the *cry1cry2* mutant exhibited a long hypocotyl phenotype. The introduction of CRY2-EGFP but not EGFP, $CRY2^{PHR}$-EGFP+T-NLS or $CRY2^{D387A}$-EGFP rescued the long hypocotyl phenotype. The hypocotyls of $CRY2^{8Cmut}$-EGFP-expressing plants were shorter than those of the *cry1cry2* mutant, yet significantly longer than those of the CRY2-EGFP-expressing plants (Figure S10A,B). The expression of $CRY2^{\Delta N538\text{-}R557}$-EGFP+T-NLS almost rescued the long hypocotyl phenotype (Figure S10A,B). We also examined the flowering time and found that the *cry1cry2* mutant exhibited a late-flowering phenotype (63 days). The expression of CRY2-EGFP rescued the late-flowering phenotype, with the plants showing an average flowering time of 33 days (line1). Plants expressing $CRY2^{\Delta N538\text{-}R557}$-EGFP+T-NLS, $CRY2^{8Cmut}$-EGFP, $CRY2^{PHR}$-EGFP+T-NLS, EGFP and $CRY2^{D387A}$-EGFP displayed the average flowering time of 35, 38, 61, 65 and 63 days, respectively (Figure 1l,m line1 and Figure S10C). These suggest that photobody formation slightly influences CRY2 blue-light-mediated hypocotyl elongation inhibition and flowering promotion. Many signal transduction proteins are recruited to CRY2 photobodies (Wang and Lin, 2020). Whether and how the recruitment and the concentration of signal transduction proteins in the CRY2 photobodies contribute to these activities remain to be further investigated.

Here, we demonstrate that two determinants influence CRY2 photobody formation and function (Figure 1n). Our research provides a framework for the investigation into the dynamic activation processes of photoreceptors and theoretical guidance for the application of CRY2 in optogenetics.

Acknowledgements

The National Key R&D Program of China (2018YFA0507700), the National Natural Science Foundation of China (31722017 and 31870753) and the Major Project of Hubei Hongshan Laboratory (2021hszd010). The China Postdoctoral Science Foundation (2020M682437 and 2021T140241) and the Postdoctoral Science Foundation of Hubei Province of China for Ling Ma.

Conflict of interest

The authors declare no competing interests.

Author contributions

P.Y. L.M. designed the experiments. L.M. performed all the experiments and wrote the manuscript. Other authors carried out analysis and experiments.

References

Ma, L., Guan, Z., Wang, Q., Yan, X., Wang, J., Wang, Z., Cao, J. *et al.* (2020) Structural insights into the photoactivation of *Arabidopsis* CRY2. *Nat. Plants*, **6**, 1432–1438.

Partch, C.L., Clarkson, M.W., Özgür, S., Lee, A.L. and Sancar, A. (2005) Role of structural plasticity in signal transduction by the cryptochrome blue-light photoreceptor. *Biochemistry*, **44**, 3795–3805.

Seong, J. and Lin, M.Z. (2021) Optobiochemistry: genetically encoded control of protein activity by Light. *Annu. Rev. Biochem.* **90**, 475–501.

Wang, Q. and Lin, C.T. (2020) Mechanisms of cryptochrome-mediated photoresponses in plants. *Annu. Rev. Plant Biol.* **71**, 23.1–23.27.

Wang, H., Yan, X., Aigner, H., Bracher, A., Nguyen, N.D., Hee, W.Y., Long, B.M. *et al.* (2019) Rubisco condensate formation by CcmM in β-carboxysome biogenesis. *Nature*, **566**, 131–135.

Wang, X., Jiang, B., Gu, L., Chen, Y., Mora, M., Zhu, M., Noory, E. *et al.* (2021) A photoregulatory mechanism of the circadian clock in *Arabidopsis*. *Nat. Plants*, **7**, 1397–1408.

Supporting information

Additional supporting information may be found online in the Supporting Information section at the end of the article.

Supplementary Figures S1–S10 Materials and Methods

